Available online at www.sciencedirect.com
ScienceDirect
Journal of Power Sources 175 (2008) 794–799
JOURNAL OF POWER SOURCES
www.elsevier.com/locate/jpowsour

Short communication

Preparation and characterization of carbon-supported PtTi alloy electrocatalysts

Errun Ding [a], Karren L. More [b], Ting He [a,*]

[a] *Honda Research Institute USA, Inc., 1381 Kinnear Road, Columbus, OH 43212, USA*
[b] *Materials Science and Technology Division, Oak Ridge National Laboratory, Oak Ridge, TN 37831, USA*

Received 17 September 2007; received in revised form 3 October 2007; accepted 4 October 2007
Available online 10 October 2007

Abstract

Carbon-supported PtTi alloy nanoparticles with well-controlled particle size, dispersity, and composition uniformity, have been synthesized by thermal decomposition and reduction of Pt and Ti precursors at elevated temperatures. The synthesized alloy nanoparticles were characterized by X-ray diffraction, high-resolution transmission electron microscopy, X-ray photoelectron spectroscopy, and energy-dispersive spectroscopy. The catalytic activities of these alloys towards molecular oxygen electro-reduction were screened by the hydrodynamic RDE technique. Among the compositions tested, $Pt_{75}Ti_{25}$ displayed the highest catalytic activity and had a twofold improvement in catalytic performance as compared to a benchmark Pt/C catalyst.
© 2007 Elsevier B.V. All rights reserved.

Keywords: PtTi; Electrocatalysts; Alloys; Oxygen reduction reaction; Nanoparticles

1. Introduction

Proton exchange membrane fuel cells (PEMFCs) are receiving increased attention worldwide as environmentally friendly power trains for transportation applications. In the search for stable and more active electrocatalysts for the oxygen reduction reaction (ORR), extensive investigations have been conducted on platinum (Pt) alloys [1–6]. Among the materials studied, platinum titanium alloys (PtTi) are promising catalyst candidates showing improved catalytic activities and good chemical stabilities [4,5]. Besides Pt and Ti being well-known for exceptional corrosion resistance in a wide range of chemical environments, the strong Lewis acid and base interaction between Pt and Ti creates a large negative enthalpy of formation resulting in strong chemical bonds between Pt and Ti in PtTi alloys [7–10]. As a result, PtTi alloys have the potential to be alternatives to pure Pt catalysts with improved catalytic activities towards the ORR and enhanced chemical stabilities.

Nanostructured materials display unique properties that are not observed in bulk materials. Important challenges in developing nanostructured materials include the ability to control particle size, monodispersity, and microcomposition uniformity. Among various recent advances developed for carbon-supported electrocatalysts [11–20], preparation of nanoparticles from low valence organometallic precursors has received great attention [21,22]. This synthesis technique allows great flexibility in selecting particle stabilizing agents (such as polymer or ligand) and reaction solvents. Furthermore, the metal precursors are easily decomposed. One notable platinum precursor is $Pt_2(dba)_3$ (dba = bis-dibenzylidene acetone). $Pt_2(dba)_3$ is stable in air (both in solid state and in solution) and can be decomposed in hydrogen or carbon monoxide atmospheres at room temperature. Monometallic and bimetallic Pt-based nanoparticles synthesized using $Pt_2(dba)_3$ have been recently reported [23–26].

In this paper, a simple method to prepare PtTi binary alloy nanoparticles of various Pt:Ti ratios using $Pt_2(dba)_3$ and titanium chloride ($TiCl_4$) as precursors is reported. The work focused on achieving controlled particle size, dispersity, and microcomposition uniformity. The fabricated nanoparticles were extensively characterized by different analytical techniques and the catalytic activities of these alloys toward molecular oxygen electro-reduction were screened using the hydrodynamic rotating disk electrode (RDE) method. Improved

* Corresponding author. Tel.: +1 614 327 4767; fax: +1 614 340 6082.
E-mail address: the@honda-ri.com (T. He).

0378-7753/$ – see front matter © 2007 Elsevier B.V. All rights reserved.
doi:10.1016/j.jpowsour.2007.10.010

catalytic performance was achieved for $Pt_{75}Ti_{25}$ alloys as compared to commercially available Pt/C catalysts.

2. Experimental

2.1. Synthesis procedure

Carbon-supported PtTi alloy nanoparticles with various Pt:Ti ratios were synthesized using $Pt_2(dba)_3$ (dba = bis-dibenzylidene acetone) and $TiCl_4(THF)_2$ precursors in tetrahydrofuran (THF) solution. The syntheses were carried out in a dry nitrogen atmosphere either using the Schlenk technique or in a glove box. $Pt_2(dba)_3$ was prepared according to a published procedure [27] and $TiCl_4(THF)_2$ (Aldrich) was used as-received. The THF solution (Aldrich) was distilled in a nitrogen atmosphere from Na/benzophenone and inserted into a glove box without exposure to air. Vulcan XC-72R (Cabot Corp.) was used as the catalyst support and was dried under vacuum at 130 °C for 12 h before being used.

The synthesis method primarily involves (i) decomposing $Pt_2(dba)_3$ and reducing $TiCl_4$ with hydrogen at elevated temperatures, and (ii) alloying of Pt and Ti at high temperatures. The Pt:Ti ratio was controlled by precursor feed ratios since no metal loss occurred during the synthesis procedure. The particle size was controlled by the alloying temperature and duration.

Appropriate amounts of $Pt_2(dba)_3$, $TiCl_4(THF)_2$, and Vulcan XC-72R were dissolved into dry THF solutions and mixed together in a glove box. The mixture was ultrasonicated for 30 min followed by stirring for an additional 12 h. The THF solution was removed slowly at room temperature by purging with N_2. The collected powders were heat-treated at temperatures ranging from 500 °C to 950 °C for 2 h in a H_2/N_2 (1:10 v/v) gas atmosphere forming PtTi alloy nanoparticles.

2.2. Characterization

2.2.1. X-ray diffraction (XRD)

The prepared PtTi alloy nanoparticles were characterized by XRD using a Bruker powder diffractometer (a combination of model D8 Discover and D8 Advance) equipped with a scintillation detector using Cu Kα radiation. The diffraction patterns were recorded from $2\theta = 25^\circ$ to $2\theta = 90^\circ$ at a scan rate of 0.02° per step and 5 s per point. The average particle size was estimated from diffraction peak broadening using Scherrer's equation.

2.2.2. Transmission electron microscopy (TEM) and energy-dispersive spectroscopy (EDS)

The morphology and size of the PtTi alloy nanoparticles were examined by high-resolution TEM using a Hitachi HF-2000 field emission gun (FEG) TEM equipped with a Thermo Scientific ultra-thin window Si(Li) EDS. The average composition of the PtTi nanoparticles, as well as the compositions of individual nanoparticles, were determined by EDS and confirmed by inductively coupled plasma-optical emission spectroscopy (ICP-OES). The nanoparticle samples for TEM–EDS analysis were prepared by dispersing the PtTi/C powders in methanol and drop-casting onto a lacey-carbon-coated copper grid followed by drying in air at room temperature.

2.2.3. Thermogravimetric analysis and differential scanning calorimetry (TGA–DSC)

Thermal analyses were performed by using a TA Instrument model SDT 2960 Simultaneous TGA–DSC. The samples were heated in air at a rate of 20 °C min^{-1} and alloy loading was calculated by the weight change after combustion of the carbon support. The alloy loadings were targeted to be close to the benchmark commercial Pt/C catalysts (∼38.5 wt% Pt) for direct comparison with a baseline catalyst system.

2.2.4. X-ray photoelectron spectroscopy (XPS)

The surface chemistries of Pt and Ti were analyzed by XPS. The spectra were acquired from an analysis area of approximately 1 mm in diameter using a monochromatic Al Kα X-ray source. Low energy resolution survey scans were obtained first to determine the existing elements. The atomic concentrations of these elements and their local chemistries were determined from higher energy resolution multiplex scans. The samples used for analysis were prepared by sprinkling the powders onto double sided tape and blowing off the excess powder with dry nitrogen.

2.3. Electrochemical analysis

Electrochemical analyses were carried out in 0.5 M H_2SO_4 electrolyte solution in a conventional three-compartment three-electrode system using a Pt mesh counter electrode, a saturated calomel reference electrode (SCE: 0.241 V versus reversible hydrogen electrode (RHE)), and a rotating disk working electrode. The working electrode (geometric surface area: 0.196 cm^2) was prepared by pipetting and uniformly distributing 15 μL of catalyst ink over the glassy carbon rotating disk electrode (RDE) tip surface. The catalyst ink was prepared by mixing 20 mg of carbon-supported PtTi alloy catalyst, 20 mL of Milli-Q ultrapure water, and 1 mL of diluted Nafion solution (5 wt%, Aldrich) with a pulse ultrasonic probe. The electrolyte solution was de-aerated with high purity argon prior to electrochemical cleaning. Saturation with high purity oxygen was performed prior to the electrocatalytic activity screening. The potentials were controlled with respect to a SCE reference electrode by a Solartron potentiostat. All hydrodynamic polarization measurements were performed under a rotation speed of 2000 rpm with a scan rate of 5 mV s^{-1} in the anodic direction. Platinum mass specific activity was used for calculating relative activity as compared to a benchmark commercial Pt/C catalyst.

3. Results and discussion

Carbon-supported PtTi alloy nanoparticle catalysts with various Pt:Ti ratios were synthesized using the wet chemistry method described in Section 2. Table 1 lists the characteristic parameters of the PtTi binary alloy nanoparticles. The ratio of Pt to Ti in the alloy product was equal to the feed ratios of $Pt_2(dba)_3$ to $TiCl_4(THF)_2$ precursors. All PtTi alloy catalyst powders heat-treated at temperatures ≤700 °C showed similar XRD patterns.

Table 1
Characteristic parameters of various PtTi binary alloy nanoparticles synthesized

Ratio of Pt:Ti	Alloying temperature (°C)	Average particle size from XRD (nm)	Loading (wt%)	Relative mass activity at 0.8 V
83:17	500	3.2	40.5	1.3
81:19	500	2.9	36.2	1.6
75:25	500	2.7	30.0	1.9
70:30	500	2.9	35.5	1.5
56:44	500	2.6	33.4	1.2
51:49	500	2.4	31.9	1.1
45:55	500	1.3	31.5	0.9
30:70	500	2.0	32.0	0.9
24:76	500	2.0	37.0	0.7
75:25	500	2.7	30.0	1.9
72:28	700	3.4	32.1	2.1
75:25	850	5.8	30.4	–
75:25	950	11.7	30.0	–

At higher alloying temperatures, a drastic influence on the structure of the alloy nanoparticles was observed. Fig. 1(a) displays a set of XRD patterns of carbon-supported $Pt_{75}Ti_{25}$ nanoparticle catalysts heat-treated at 500 °C, 700 °C, 850 °C, and 950 °C. The XRD patterns for the 500 °C- and 700 °C-treated alloy nanoparticles predominately display the Pt face-centered cubic (fcc) structure (PDF card #04-0802). The peak assignments are

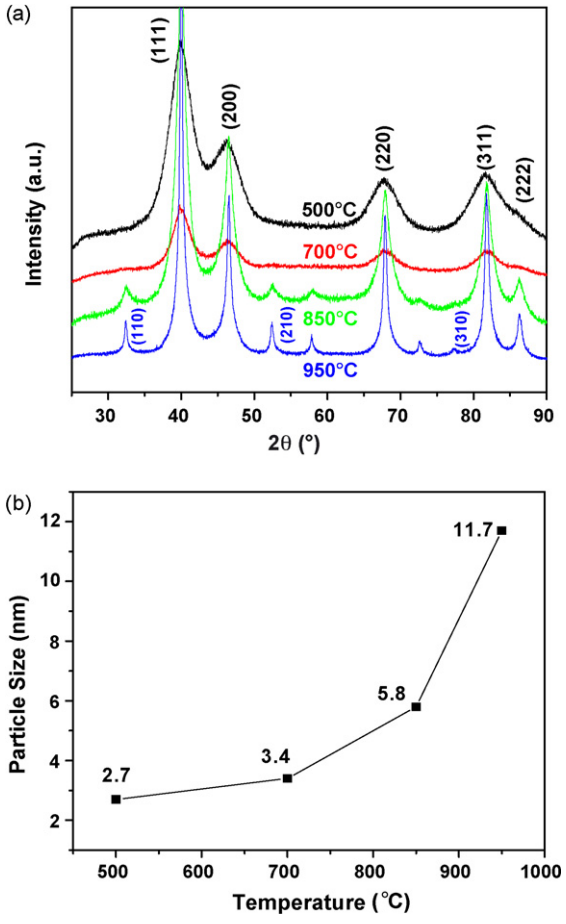

Fig. 1. (a) XRD patterns of carbon-supported $Pt_{75}Ti_{25}$ nanoparticles heat-treated at 500 °C, 700 °C, 850 °C, and 950 °C; (b) the corresponding nanoparticle sizes determined from XRD (2 2 0) peak broadening.

Pt (1 1 1), (2 0 0), (2 2 0), (3 1 1), and (2 2 2) reflections. At the higher alloying temperatures of 850 °C and 950 °C, the ordered Pt_3Ti $L1_2$ intermetallic structure formed as indicated by the presence of the [1 0 0], [1 1 0], and [1 1 1] superlattice diffraction peaks (PDF card #17-0064; only [1 1 0] superlattice diffraction peaks were labeled for simplicity). No secondary phases were identified by XRD in the PtTi alloy nanoparticles indicating that the majority of the titanium was alloyed with platinum. Fig. 1(b) displays the particle size of the carbon-supported $Pt_{75}Ti_{25}$ alloy nanoparticles as a function of heat treatment (alloying) temperature. The average particle size, calculated from broadening of the (2 2 0) peak in the XRD data, increased gradually with alloying temperatures from 500 °C to 700 °C (2.7–3.4 nm) whereas the higher alloying temperatures of 850 °C and 950 °C resulted in rapid particle growth (5.8 nm and 11.7 nm).

Fig. 2(a) shows a representative TEM image of a carbon-supported PtTi alloy nanoparticle catalyst. The alloy nanoparticles were alloyed at 500 °C for 2 h in a H_2/N_2 (1:10 v/v) gas mixture. In the TEM image, the PtTi nanoparticles appear as dark spots on the carbon support. All PtTi alloys (see Table 1) display spherical PtTi nanoparticles that are uniformly dispersed on the carbon-support. The nanoparticle sizes ranged from 1 nm to 4 nm with a narrow particle size distribution as determined by particle size analyses from TEM images such as the one shown in Fig. 2(b). The results agreed well with the XRD particle size analyses. High-magnification TEM was used to characterize the atomic structure of individual PtTi nanoparticles, Fig. 2(c), and the results indicated that the alloy nanoparticles were well-crystallized. The XRD and TEM results clearly demonstrate that the synthesis method developed here is extremely effective for synthesizing small and uniformly dispersed crystalline PtTi alloy nanoparticle catalysts.

The surface chemistries of Pt and Ti associated with the PtTi alloy nanoparticle catalysts were characterized by XPS. The alloy nanoparticle catalysts showed varying concentrations of carbon, oxygen, platinum, and titanium. The main differences between the alloys were the amount of oxygen present and the platinum chemistries. Fig. 3 displays a representative Pt 4f X-ray photoelectron spectrum measured on a carbon-supported $Pt_{75}Ti_{25}$ alloy nanoparticle catalyst. The spectrum displays the

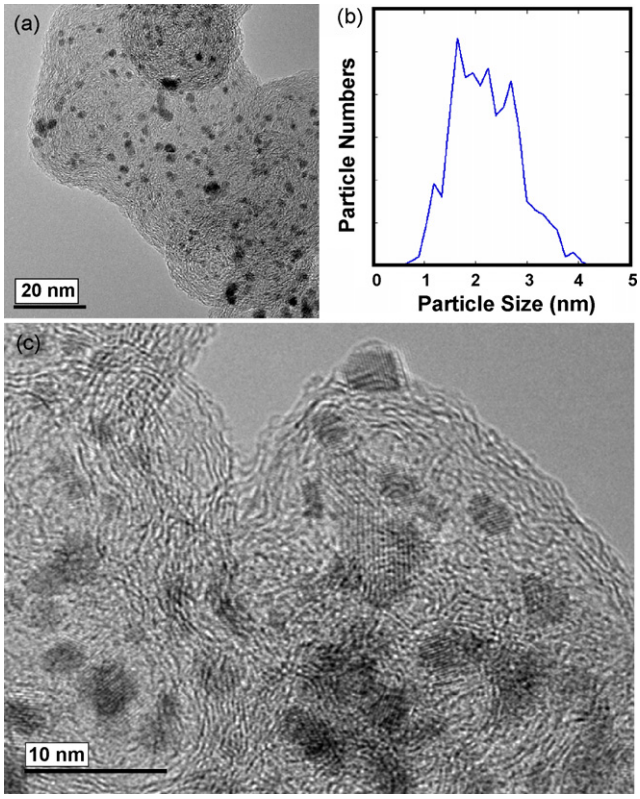

Fig. 2. (a) TEM image of a carbon-supported PtTi nanoparticle catalyst heat-treated at 500 °C; (b) the corresponding particle size distribution; (c) high-resolution TEM image of a carbon-supported PtTi nanoparticles showing the lattice fringes.

typical Pt $4f_{7/2}$ and $4f_{5/2}$ doublet separated by 3.33 eV (data in black). Least-square fitting of the Pt 4f doublet reveals three binding energies: 71.7 eV (red), 72.9 eV (blue), and 74.8 eV (gray), for the Pt $4f_{7/2}$ peak, and the corresponding intensities (concentrations). The binding energy of 71.7 eV is higher than the measured binding energies of zero-valent Pt from bulk (70.8 eV) and nanoparticles (70.6 eV) [28], but is almost identical to the Pt binding energy for an intermetallic Pt_3Ti alloy (71.5 eV) documented in the National Institute of Standards & Technology (NIST) XPS database [29]. Therefore, the Pt 71.7 eV binding energy may be assigned to the Pt $4f_{7/2}$ signal from the intermetallic compound Pt_3Ti. The assignment of the signal at 72.9 eV is uncertain. Though it was assigned to PtO in literature [28], the intensity of this peak (15–35%) reported in literatures [28,30] is too high for pure Pt. Even after heat-treating in a hydrogen atmosphere at temperatures as high as 950 °C, the signal intensity remained 20% of the total concentration in the PtTi powders. Additionally, the PtO signal should be close to 74.0 eV [29]. Hence, the Pt peak at 72.9 eV is suspected to arise from $Pt(OH)_2$ since the formation enthalpy of $Pt(OH)_2$ is less than that of PtO_2 or Pt organometallic compounds. The last binding energy peak at 74.8 eV agrees well with PtO_2 and is only a few percent in intensity.

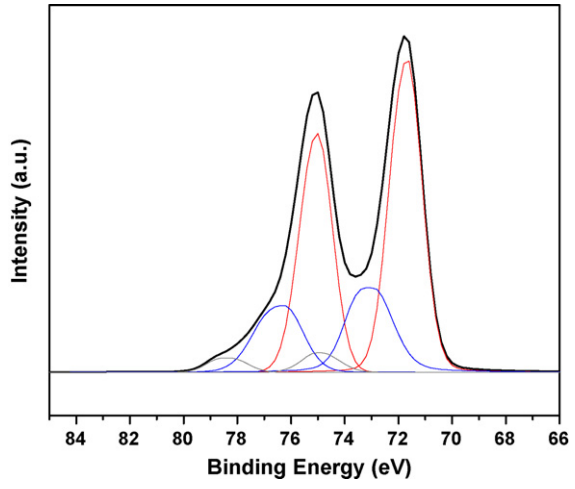

Fig. 3. XPS analysis of Pt $4f_{7/2}$ binding energy of carbon-supported $Pt_{75}Ti_{25}$ nanoparticles. (For interpretation of the references to color in text, the reader is referred to the web version of the article.)

The concentration of the Pt_3Ti intermetallic alloy did not increase as much as expected (from 62% to 76%) with increasing alloying temperatures from 500 °C to 950 °C. Since XRD patterns for $Pt_{75}Ti_{25}$ alloy nanoparticle catalysts heat-treated at 500 °C or 700 °C do not show the formation of the ordered Pt_3Ti structure, the observation of the Pt_3Ti intermetallic structure by XPS is likely from the presence of Pt–Ti intermetallic type bonding and not necessarily from the formation of an ordered structure. This Pt–Ti bonding may contribute to the superior catalytic activities of $Pt_{75}Ti_{25}$ alloy nanoparticles as will be discussed later. Moreover, even though the XPS signals of Ti $2p_{3/2}$ and $2p_{1/2}$ were very weak, intermetallic Ti was observed to increase with increasing alloying temperature.

Fig. 4(a) displays a representative micro-compositional analysis of individual PtTi nanoparticles by high spatial resolution EDS performed in TEM mode. The experiments were performed using a probe diameter of ~1.5 nm. The results of EDS analyses showed differences in the Pt:Ti ratio as a function of alloy particle size as shown in Fig. 4(b). The micro-compositions of individual PtTi nanoparticles were relatively uniform with the Ti content varying between 14% and 21%; however, smaller particles tended to contain less Ti than larger particles. The composition difference may explain the relatively lower performance of PtTi nanopowders as compared to thin alloy films [4,5] indicating a need for even better micro-composition uniformity. Overall, the micro-composition uniformity for PtTi alloy nanoparticles was fairly good in comparison to other binary alloy nanoparticles synthesized by conventional methods.

The catalytic activities towards molecular oxygen electron-reduction were measured by the hydrodynamic RDE technique. Fig. 5(a) shows a representative hydrodynamic polarization curve of a carbon-supported $Pt_{75}Ti_{25}$ alloy nanoparticle catalyst (solid line, 30 wt% alloy) as compared to a benchmark Pt/C catalyst (dashed line, 38.5 wt% Pt) under the exact same testing conditions. The results clearly show that the prepared $Pt_{75}Ti_{25}$ catalyst is more active than the benchmark Pt/C catalyst. A twofold increase in mass specific activity (or a 20 mV shift to higher potential) is observed. Fig. 5(b) displays the relative mass specific activities for various carbon-supported PtTi alloy nanoparticle catalysts as compared to a benchmark Pt/C catalyst. A standard volcano type plot was observed where enhanced

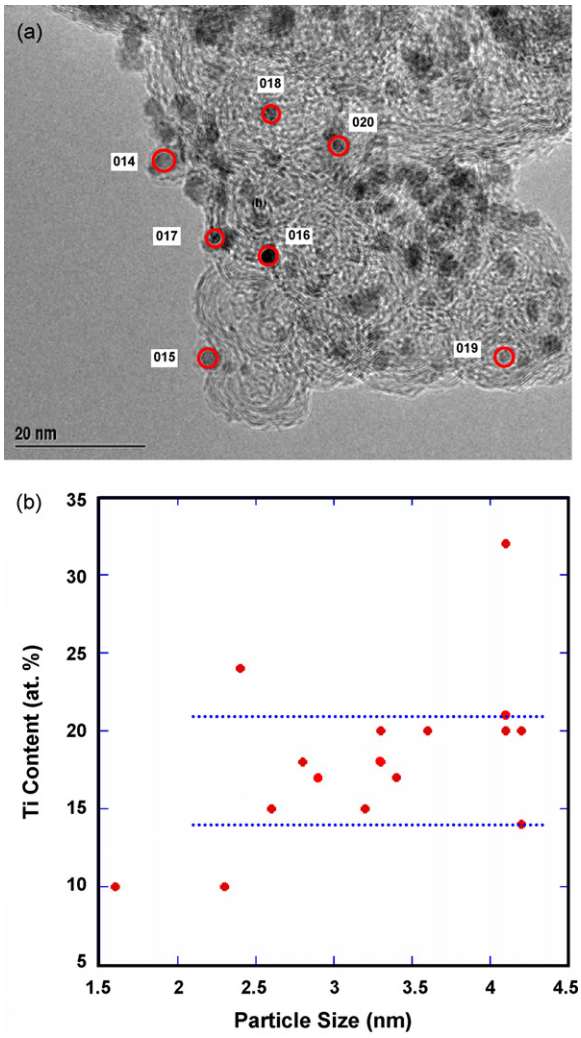

Fig. 4. (a) High spatial resolution TEM–EDS analysis of micro-compositions of individual PtTi nanoparticles; (b) the Ti atomic concentration of individual PtTi nanoparticles as a function of particle size.

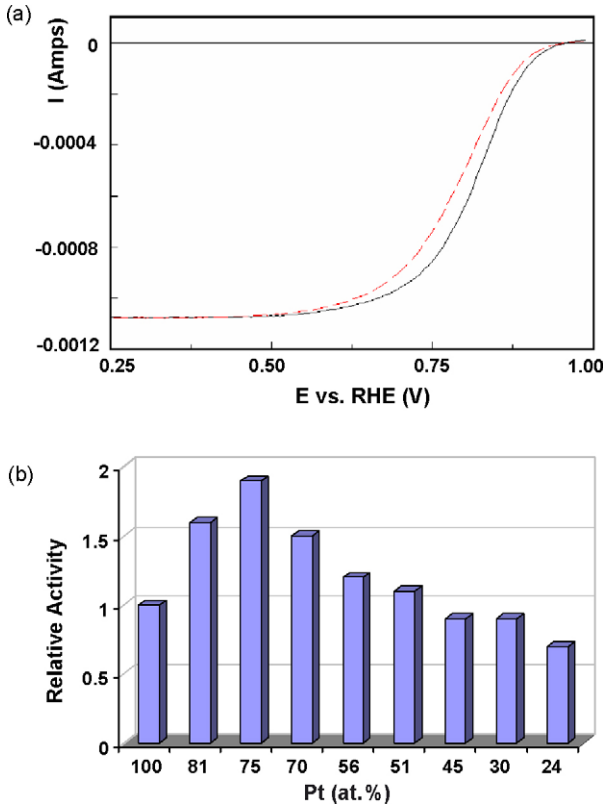

Fig. 5. (a) Hydrodynamic polarization curve of carbon-supported $Pt_{75}Ti_{25}$ nanoparticles (solid line, 30 wt% alloy) compared to a standard commercial Pt/C catalyst (dashed line, 38.5 wt% Pt); (b) relative mass specific activities of carbon-supported PtTi catalysts of various compositions compared to a standard commercial Pt/C catalyst. All PtTi nanoparticle powders were heat-treated at 500 °C.

catalytic performance was found for PtTi alloys with Pt concentrations of 50 at.% or higher with the catalytic activity peaking at 75 at.% Pt. The nanoparticle results match the thin film-based high-throughput discovery results where a similar volcano shape and performance levels were found [5].

Similar to other well-known Pt binary alloys that utilize 3d transition metals as the alloying element, the catalytic performance of PtTi alloy catalysts is very sensitive to the Pt:Ti atomic ratio with the activity dropping as the composition shifts away from the optimum Pt:Ti atomic ratio of 75:25. Similarly, a sharp drop in performance was observed in our thin film work with a small compositional shift away from the optimized ratio [5]. At present, it is still not clear whether or not the Pt_3Ti intermetallic compound is more active towards the ORR than the solid solution phase. A systematic study needs to be conducted to determine the effects of atomic order/disorder on catalytic activity in these binary alloy catalysts, where further synthesis research is necessary to create the two different phases with similar particle size and dispersity for comparison.

The mechanisms for catalytic enhancement of platinum alloys have been studied extensively and various possible reasons have been proposed [31–37] including the role of alloy d-band centers, modification of platinum d-band vacancies, Pt–Pt interatomic distances, the effect of alloy facets, surface roughening due to leaching out of non-precious elements, and improved wettability. The volcano type plot of activity versus composition shown in Fig. 5(b) indicates there could be an optimal d-band vacancy in Pt leading to a maximum in activity [31]. The Ti atoms may function as adsorption sites for chemisorbed OH^-_{ad} and O_2 in the dissociative adsorption of O_2 as observed in other transition metals [38]. This could influence the coverage of OH^- or O_2 on the surface of catalysts and hence the catalytic activity.

4. Conclusion

Carbon-supported PtTi binary alloy nanoparticles with various compositions have been synthesized. Small particle sizes with narrow size distributions were achieved. XRD results show that the $Pt_{75}Ti_{25}$ catalyst particles are dominated by the Pt_3Ti intermetallic structure when heat-treated at temperatures of 850 °C or greater. Higher catalytic performance towards molecular oxygen electro-reduction was found for PtTi alloys with Pt concentration of 50 at.% or greater. The peak catalytic activity

was found for $Pt_{75}Ti_{25}$, displaying a twofold increase in activity, or a 20 mV shift to higher potential, as compared to a benchmark Pt/C catalyst.

Acknowledgments

Part of this research was supported by the U.S. Department of Energy, Office of Hydrogen, Fuel Cells, and Infrastructure Technologies, as part of contract DE-AC05-00OR22725 with UT-Battelle, LLC. The authors acknowledge Eric Kreidler for kind assistance in preparing the manuscript.

References

[1] B.C. Beard, P.N. Ross, J. Electrochem. Soc. 137 (1990) 3368–3374.
[2] V.R. Stamenkovic, B. Fowler, B.S. Mun, G. Wang, P.N. Ross, C.A. Lucas, N.M. Markovic, Science 315 (2007) 493–497.
[3] M. Watanabe, K. Tsurumi, T. Mizukami, T. Nakamura, P. Stonehart, J. Electrochem. Soc. 141 (1994) 2659–2668.
[4] T. He, E. Kreidler, L. Xiong, J. Luo, C.J. Zhong, J. Electrochem. Soc. 153 (2006) A1637–A1643.
[5] T. He, E. Kreidler, L. Xiong, E. Ding, J. Power Sources 165 (2007) 87–91.
[6] T.R. Ralph, M.P. Hogarth, Platinum Met. Rev. 46 (2002) 3–14.
[7] E. Ellner, J. Alloy Compd. 336 (2004) 222–227.
[8] Q. Guo, O.J. Kleppa, J. Alloy Compd. 321 (2001) 169–182.
[9] Q. Guo, O.J. Kleppa, J. Alloy Compd. 256 (1998) 224–229.
[10] L. Brewer, Acta Metall. 15 (1967) 553–555.
[11] T. He, in: P.D. Cozzoli (Ed.), Recent Advances in Solution-based Chemical Synthesis of Semiconductor, Metal, and Oxide Nanocrystals, Research Signpost, in press.
[12] J. Luo, L. Han, N.N. Kariuki, L. Wang, D. Mott, C.J. Zhong, T. He, Chem. Mater. 17 (2005) 5282–5290.
[13] J. Luo, N. Kariuki, L. Han, L. Wang, C.-J. Zhong, T. He, Electrochim. Acta 51 (2006) 4821–4827.
[14] J. Luo, L. Wang, D. Mott, P.N. Njoki, N. Kariuki, C.-J. Zhong, T. He, J. Mater. Chem. 16 (2006) 1665–1673.
[15] L. Xiong, T. He, Chem. Mater. 18 (2006) 2211–2218.
[16] L. Xiong, T. He, Electrochem. Commun. 8 (2006) 1671–1676.
[17] J.D. Graaf, A.J.V. Dillen, K.P.D. Jong, D.C. Koningsberger, J. Catal. 203 (2001) 307–321.
[18] N. Tian, Z.-Y. Zhou, S.-G. Sun, Y. Ding, Z.L. Wang, Science 316 (2007) 732–735.
[19] J. Chen, T. Herricks, Y. Xia, Angew. Chem. Int. Ed. 44 (2005) 2589–2592.
[20] N. Alonso-Vante, Fuel Cells 6 (2006) 182–189.
[21] C.W. Scheeren, G. Machado, S.R. Teixeira, J. Morais, J.B. Domingos, J. Dupont, J. Phys. Chem. B 110 (2006) 13011–13020.
[22] C.W. Scheeren, G. Machado, J. Dupont, P.F.P. Fichtner, S.R. Teixeira, Inorg. Chem. 42 (2003) 4738–4742.
[23] S. Gomez, L. Erades, K. Philippot, B. Chaudret, V. Collière, O. Balmesb, J.-O. Bovin, Chem. Commun. (2001) 1474–1475.
[24] T.O. Ely, C. Pan, C. Amiens, B. Chaudret, F. Dassenoy, P. Lecante, M.-J. Casanove, A. Mosset, M. Respaud, J.-M. Broto, J. Phys. Chem. B 104 (2000) 695–702.
[25] C. Pan, F. Dassenoy, M.-J. Casanove, K. Philippot, C. Amiens, P. Lecante, A. Mosset, B. Chaudret, J. Phys. Chem. B 103 (1999) 10098–10101.
[26] A. Duteil, R. Quhau, B. Chaudret, R. Maze, C. Roucau, J.S. Bradley, Chem. Mater. 5 (1993) 341–347.
[27] K. Moseley, P.M. Maitlis, J. Chem. Soc. Chem. Commun. (1971) 982–983.
[28] A.K. Shukla, M. Neergat, P. Bera, V. Jayaram, M.S. Hegde, J. Electroanal. Chem. 504 (2001) 111–119.
[29] NIST X-ray Photoelectron Spectroscopy Database, NIST Standard Reference Database 20, version 3.4 (web version), srdata.nist.gov/xps.
[30] A. Seo, J. Lee, K. Han, H. Kim, Electrochim. Acta 52 (2006) 1603–1611.
[31] A. Ruban, B. Hammer, P. Stoltze, H.L. Skriver, J.K. Norskov, J. Mol. Catal. A 115 (1997) 421–429.
[32] S. Mukerjee, S. Srinivasan, M.P. Soriaga, J. McBreen, J. Electrochem. Soc. 142 (1995) 1409–1415.
[33] V.M. Jalan, US Patent 4,202,934 (1980).
[34] M.T. Paffett, J.G. Beery, S. Gottesfeld, J. Electrochem. Soc. 135 (1988) 1431–1437.
[35] V. Stamenkovic, T.J. Schmidt, P.N. Ross, N.M. Markovic, J. Phys. Chem. B 106 (2002) 11970–11979.
[36] L. Xiong, A. Manthiram, J. Mater. Chem. 14 (2004) 1454–1460.
[37] H.A. Gasteiger, S.S. Kocha, B. Sompalli, F.T. Wagner, Appl. Catal. B 56 (2005) 9–35.
[38] H. Yamazaki, S. Kamimizu, K. Hara, K. Sakamoto, Surf. Sci. 538 (2003) L505–L510.